

## Supporting Information: Surface Plasmon Modes of Nanomesh-on-Mirror

### Nanocavities Prepared by Nanosphere Lithography

Christian Stelling,<sup>1</sup> Stefan Fossati,<sup>2</sup> Jakub Dostalek,<sup>2\*</sup> Markus Retsch<sup>1\*</sup>

<sup>1</sup> Department of Chemistry, University of Bayreuth, 95447 Bayreuth, Germany

<sup>2</sup> Biosensor Technologies, AIT-Austrian Institute of Technology GmbH, Konrad-Lorenz-Strasse 24 | 3430 Tulln,  
Austria

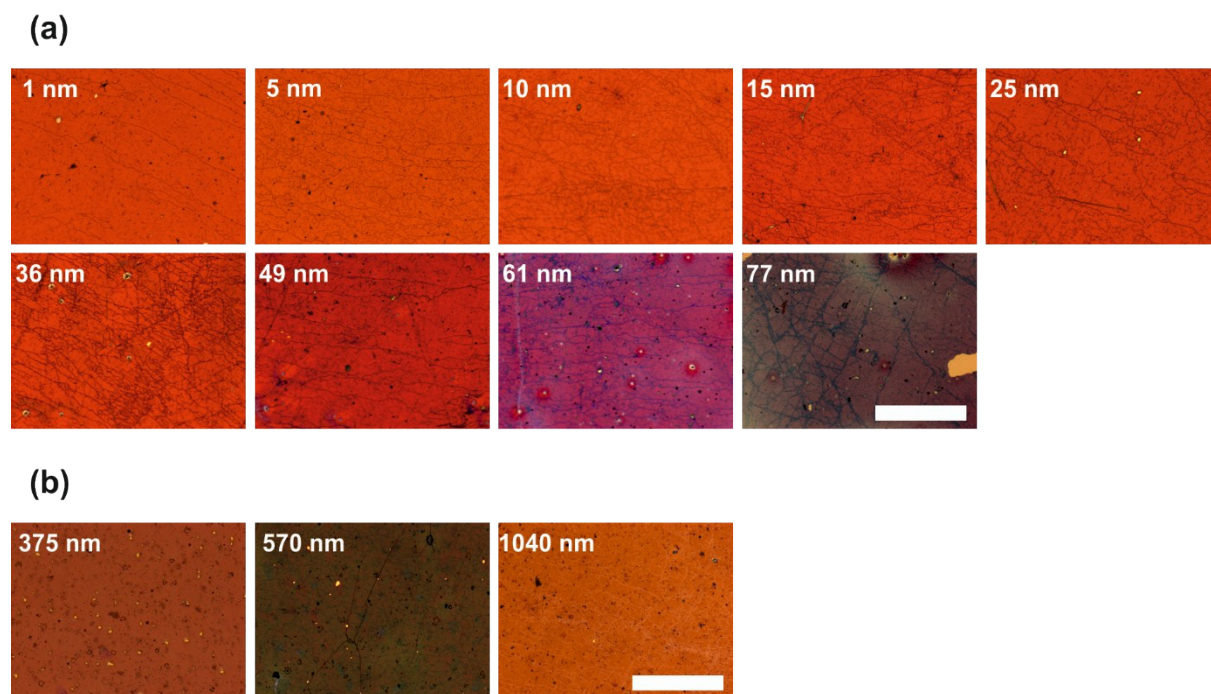


**Figure S1.** Optical microscopy images of MIM structures with (a) distinct spacer thicknesses and (b) distinct lattice periods. Scale bars are 500  $\mu\text{m}$ .

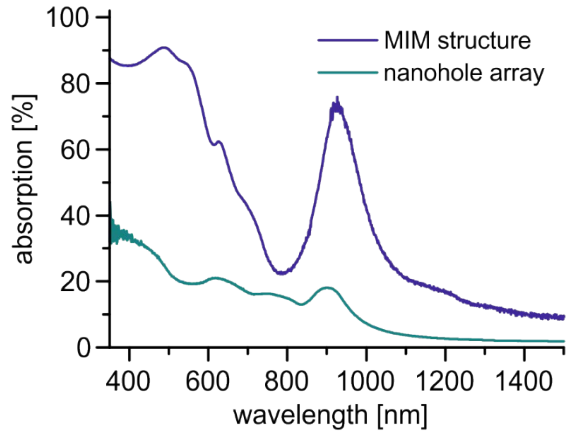


**Figure S2.** Measured absorption (1-reflectance) of a MIM structure with  $p = 570$  nm,  $t_{\text{gold}} = 100$  nm,  $t_{\text{gap}} = 50$  nm and  $t_{\text{hole}} = 90$  nm compared to an isolated gold nanohole array with  $p = 570$  nm.

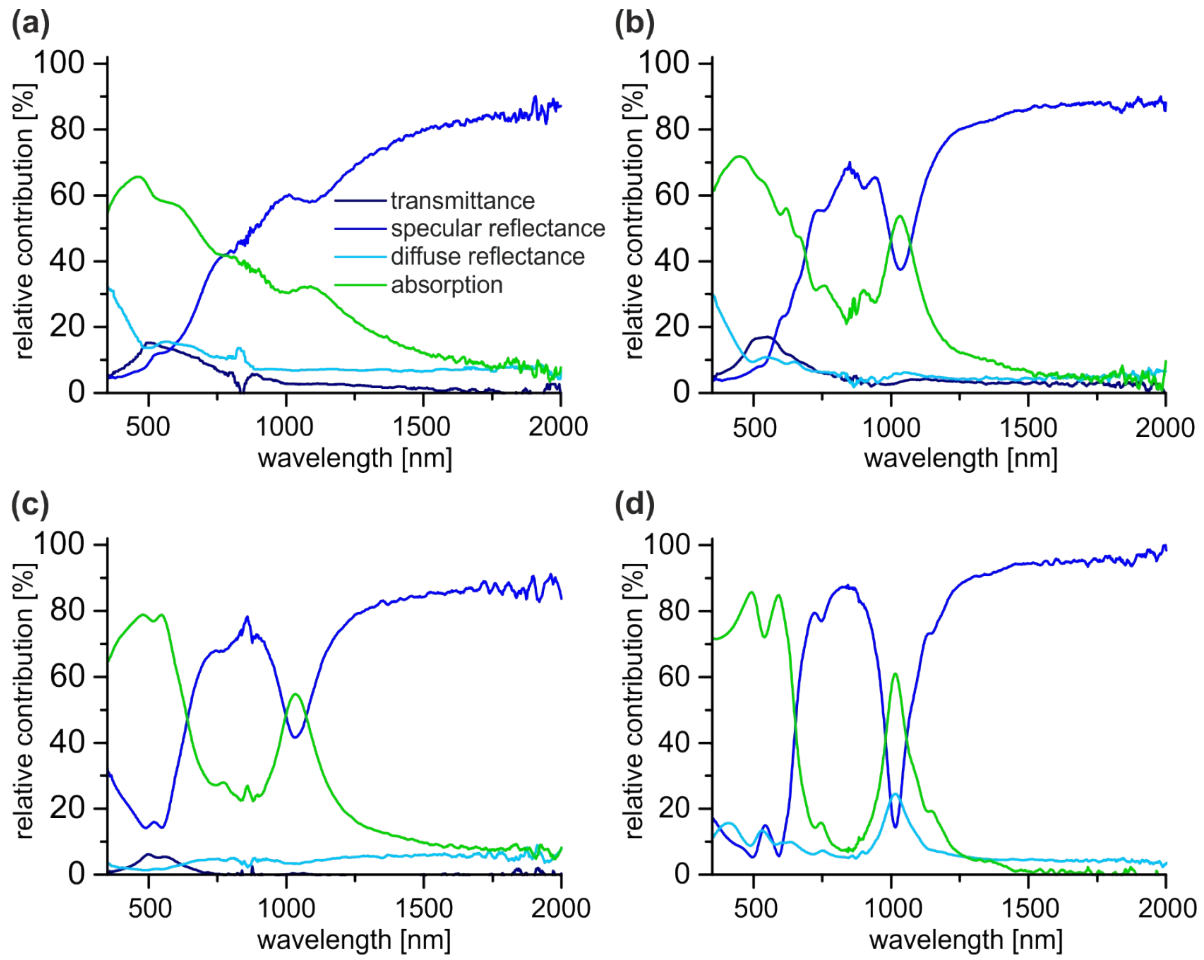


**Figure S3.** Influence mirror thickness. Transmittance, specular reflectance, diffuse reflectance and absorption for MIM structures with  $p = 570$  nm,  $t_{\text{gap}} = 30$  nm,  $t_{\text{hole}} = 80$  nm and (a)  $t_{\text{gold}} = 13$  nm (b)  $t_{\text{gold}} = 21$  nm (c)  $t_{\text{gold}} = 40$  nm (d)  $t_{\text{gold}} = 100$  nm.

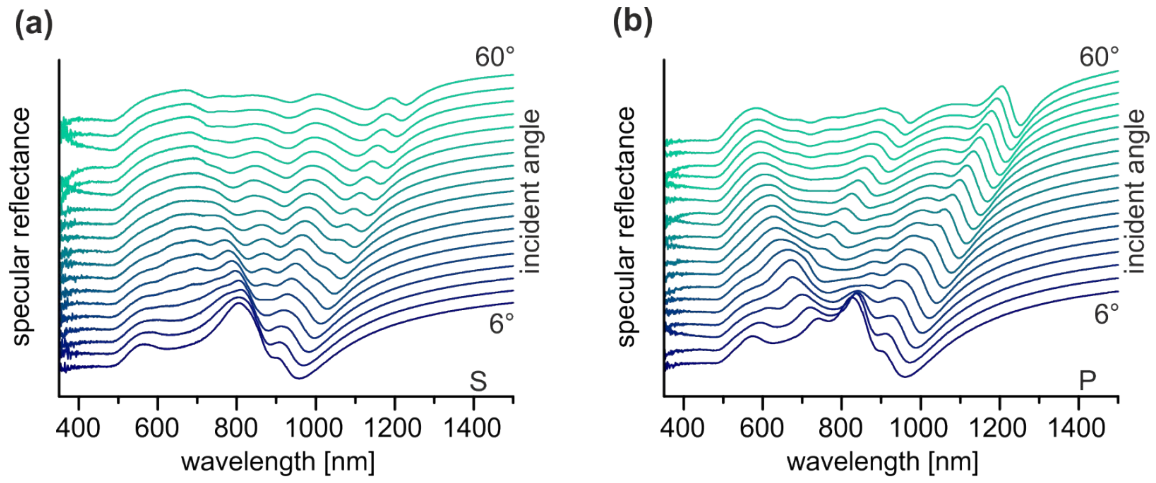


**Figure S4.** Angle-resolved reflectance measurements with (a) s-polarized and (b) p-polarized light of an isolated gold nanohole array with  $p = 570$  nm.

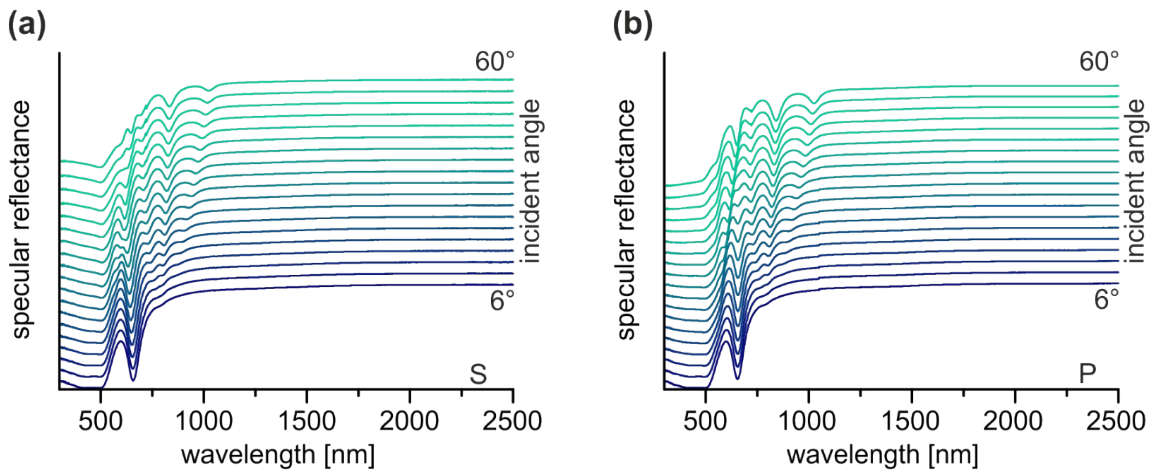


**Figure S5.** Angle-resolved reflectance measurements with (a) s-polarized and (b) p-polarized light of a MIM structure with  $p = 375$  nm,  $t_{\text{gold}} = 100$  nm,  $t_{\text{gap}} = 40$  nm and  $t_{\text{hole}} = 90$  nm.

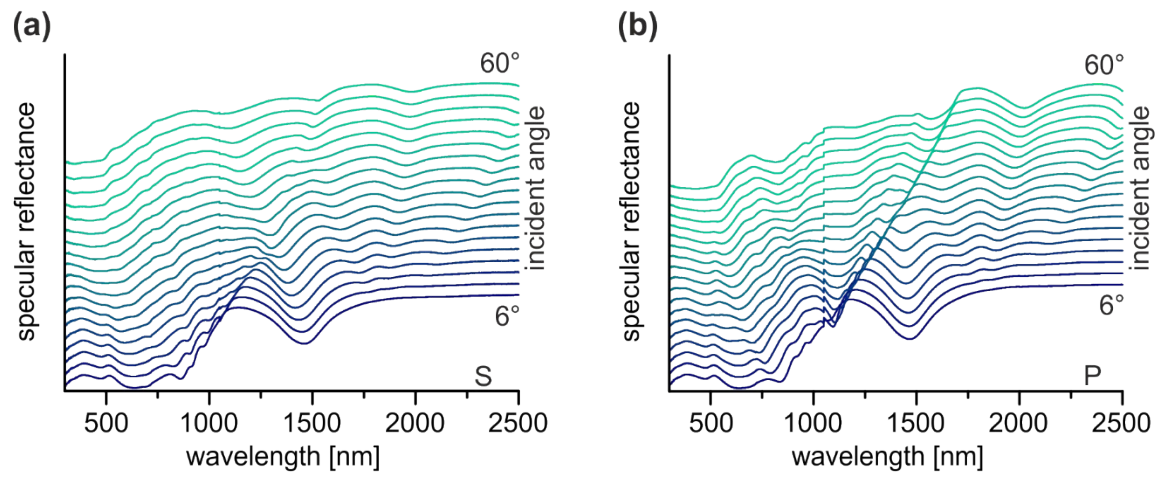


**Figure S6.** Angle-resolved reflectance measurements with (a) s-polarized and (b) p-polarized light of a MIM structure with  $p = 1040$  nm,  $t_{\text{gold}} = 100$  nm,  $t_{\text{gap}} = 40$  nm and  $t_{\text{hole}} = 90$  nm.

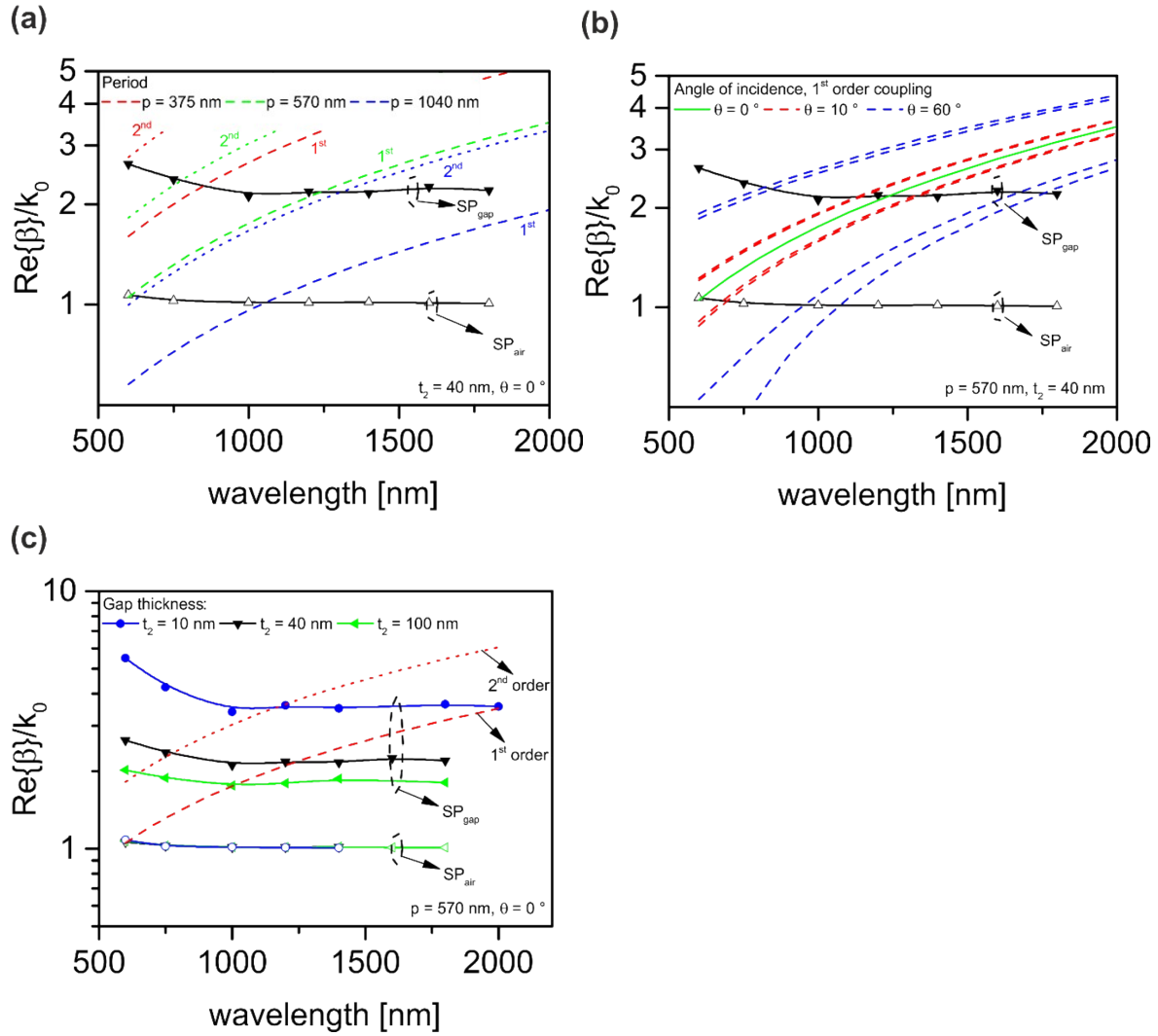


**Figure S7.** Analytically derived dispersion curves of the two SPP modes present in the MIM structures. (a) Influence of the lattice period at normal incidence. (b) Influence of the angle of incidence for  $p = 570$  nm. Assumed coupling via all (0,1), (1,0), (1,1), (0,1), (1,0) and (1,1) orders. The plane of incidence was assumed to be parallel with (0,1) and (0,1) orders. (c) Influence of the spacer thickness for  $p = 570$  nm at normal incidence.  $\beta$  is the propagation constant of guided modes,  $k_0$  is the light wavenumber in vacuum.

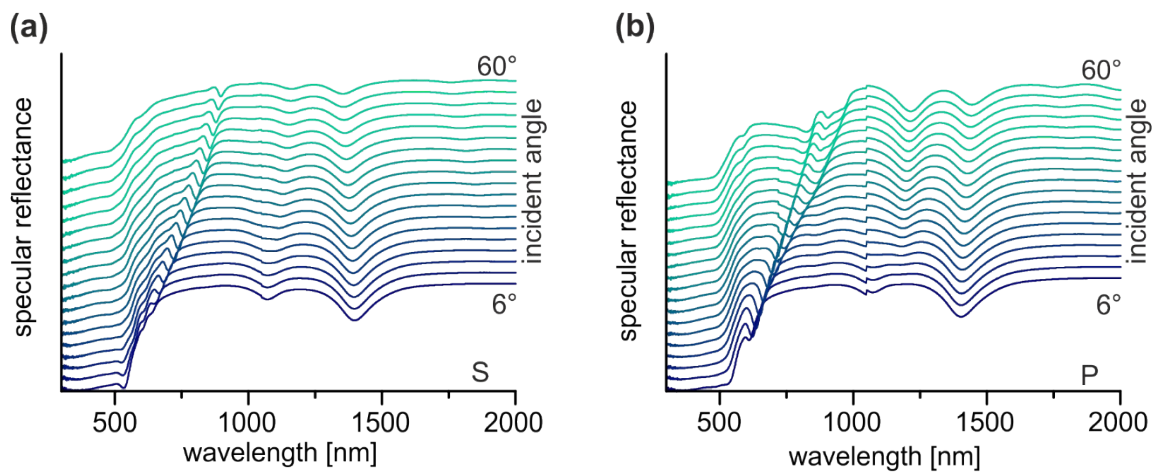


**Figure S8.** Angle-resolved reflectance measurements with (a) s-polarized and (b) p-polarized light of a MIM structure with  $p = 570$  nm,  $t_{\text{gold}} = 100$  nm,  $t_{\text{gap}} = 1$  nm and  $t_{\text{hole}} = 90$  nm.

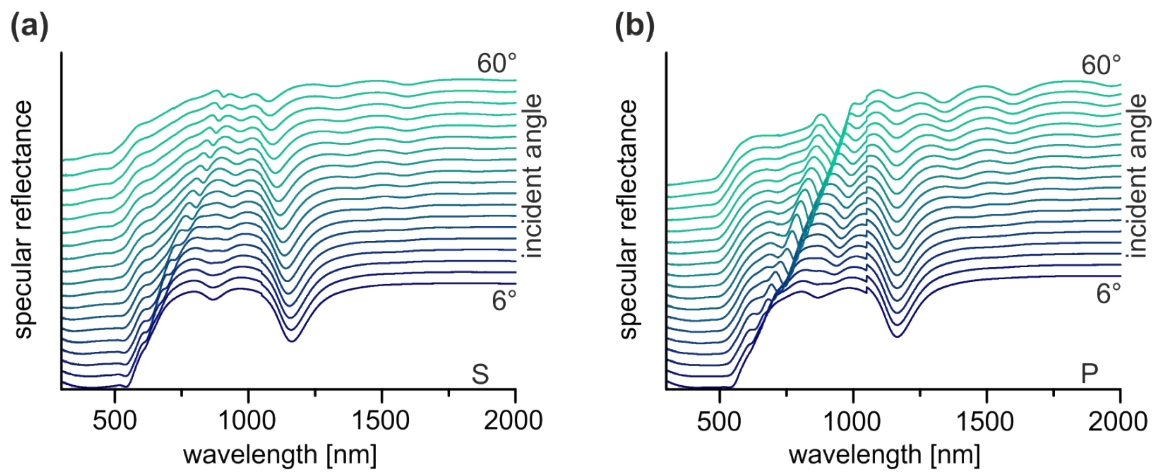


**Figure S9.** Angle-resolved reflectance measurements with (a) s-polarized and (b) p-polarized light of a MIM structure with  $p = 570$  nm,  $t_{\text{gold}} = 100$  nm,  $t_{\text{gap}} = 15$  nm and  $t_{\text{hole}} = 90$  nm.

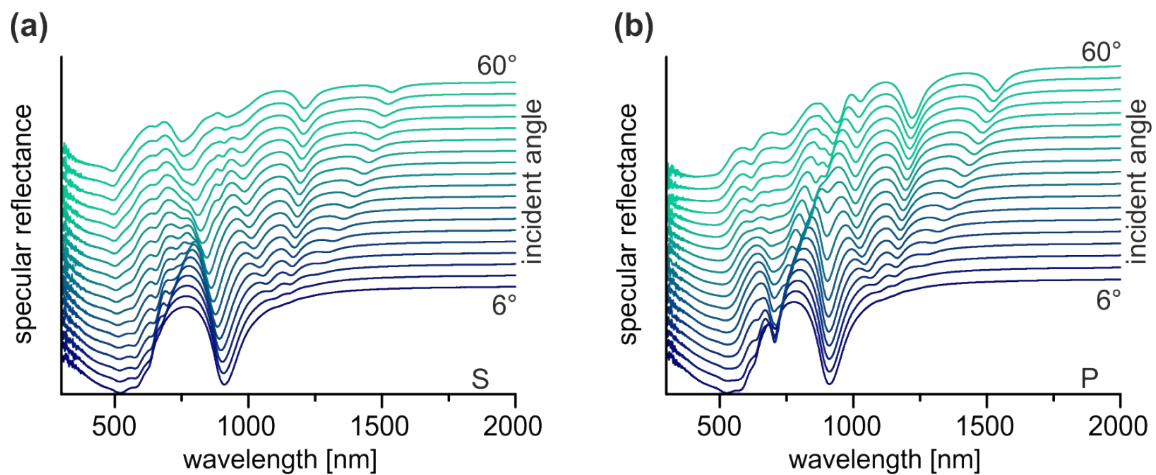


**Figure S10.** Angle-resolved reflectance measurements with (a) s-polarized and (b) p-polarized light of a MIM structure with  $p = 570$  nm,  $t_{\text{gold}} = 100$  nm,  $t_{\text{gap}} = 50$  nm and  $t_{\text{hole}} = 90$  nm.



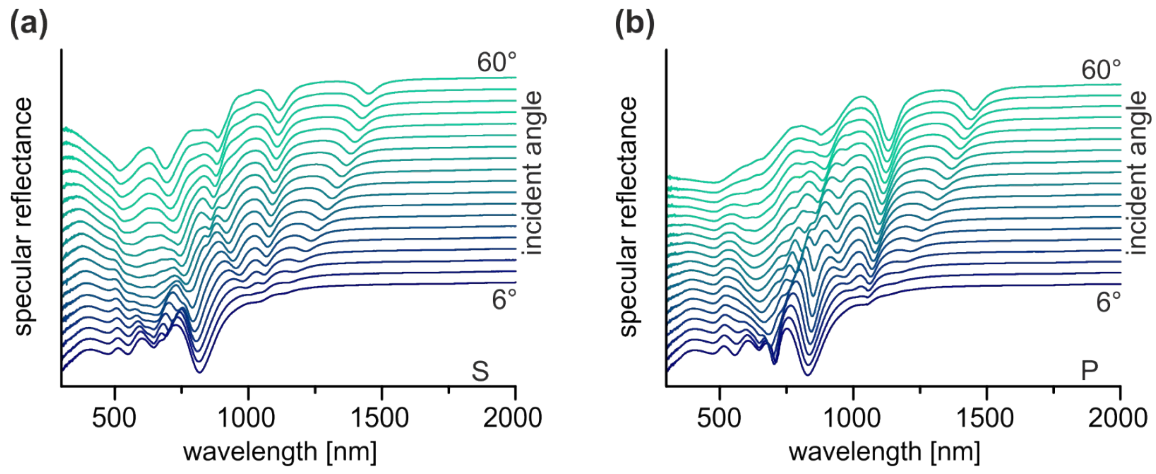


**Figure S11.** Angle-resolved reflectance measurements with (a) s-polarized and (b) p-polarized light of a MIM structure with  $p = 570$  nm,  $t_{\text{gold}} = 100$  nm,  $t_{\text{gap}} = 77$  nm and  $t_{\text{hole}} = 90$  nm.

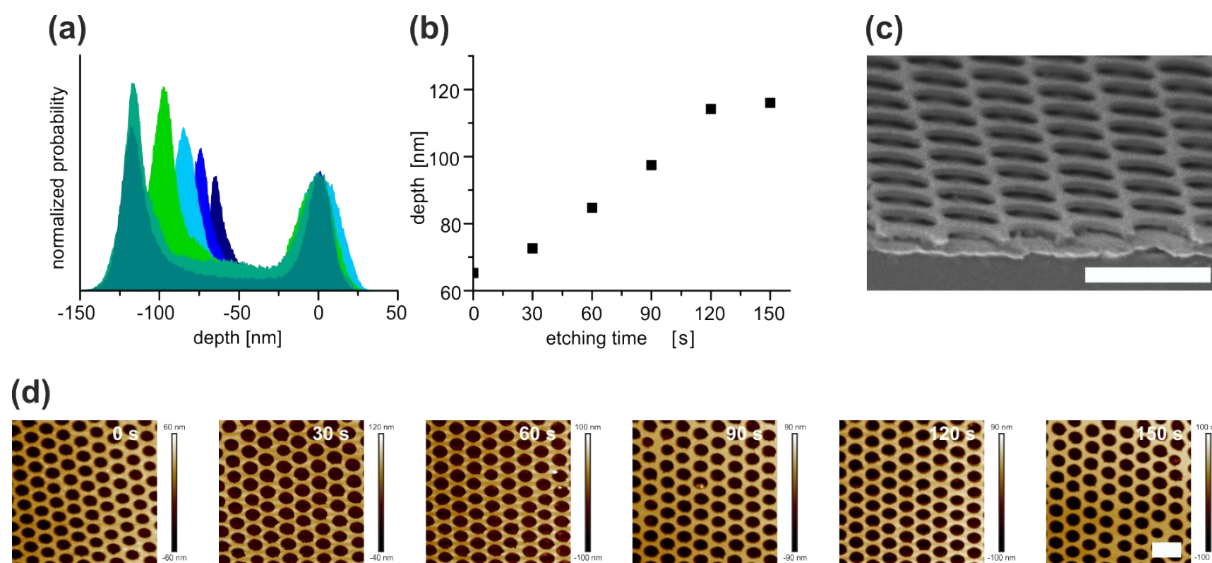


**Figure S12.** Plasma etching of MIM structure. (a) Depth profile of the MIM structure measured with AFM after consecutive etching steps. (b) Depth of the plasma etched MIM structure with increasing etching time. (c) Side-view SEM image of the MIM structure etched for 150 s. (d) AFM images of the MIM structure after each etching step, Scale bars are 1  $\mu\text{m}$ .

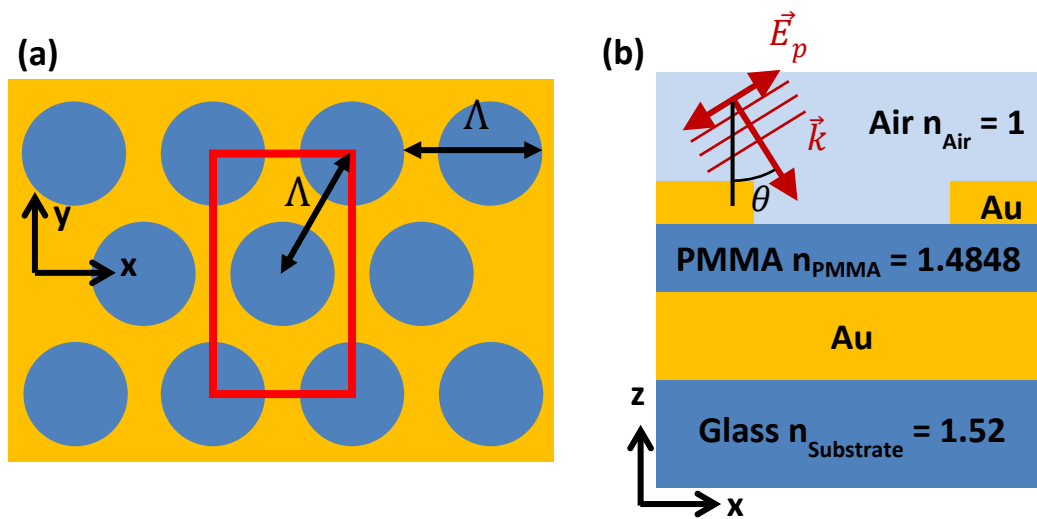


**Figure S13.** Schematic of geometry used in FDTD simulation for hexagonal nanomeshes with a rectangular unit cell. (a) Top view. The red rectangle indicates simulation volume with Bloch boundary conditions. A vertical cross-section is shown in (b) with the definition of the angle of incidence  $\theta$  and E-field orientation  $E_0$  for p-polarization.

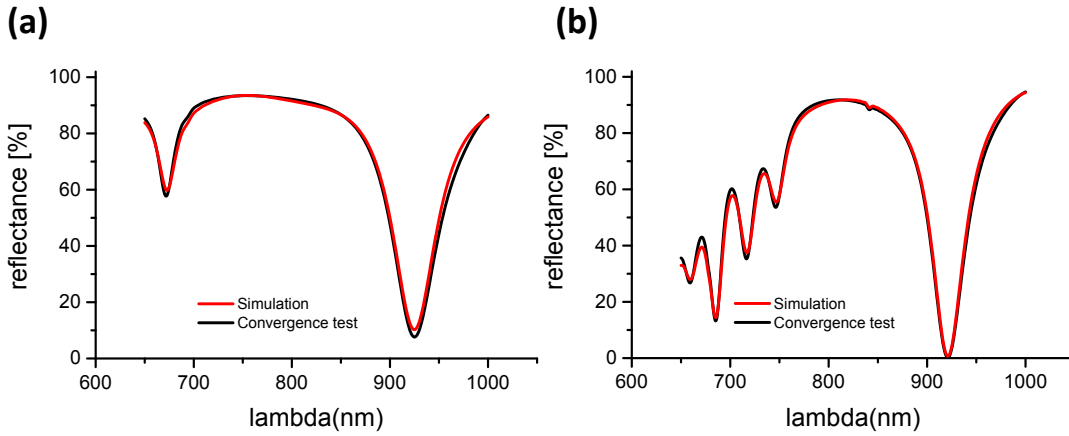


**Figure S14.** Convergence of the simulation was tested by increase of the mesh resolution. Simulations were run with a uniform mesh of  $(x,y,z) = (5 \text{ nm}, 5 \text{ nm}, 2 \text{ nm})$  unit cell size. The Mesh size was reduced to  $(x,y,z) = (2 \text{ nm}, 2 \text{ nm}, 2 \text{ nm})$  for selected configurations to confirm the convergence of results. Here, the convergence test for the shorter wavelength part of the spectrum is shown for the geometry used to study near-field distribution in Figure 4 for (a) normal incident light and (b) excitation with  $\theta = 22^\circ$  angle of incidence.